

Model Independent Analysis of Interactions between Dark Matter and Various Quarks

Biplob Bhattacharjee^(a), Debajyoti Choudhury^(b), Keisuke Harigaya^(a),
Shigeki Matsumoto^(a) and Mihoko M. Nojiri^(c,a)

^(a) *Kavli IPMU, University of Tokyo, Kashiwa, 277-8583, Japan*

^(b) *Department of Physics and Astrophysics,
University of Delhi, Delhi 110007, India.*

^(c) *Theory Group, KEK, Tsukuba, 305-0801, Japan*

Abstract

Present and future expected limits on interactions between dark matter and various quarks are thoroughly investigated in a model-independent way. In particular, the constraints on the interactions from the Large Hadron Collider (LHC) experiment are carefully considered with focusing on mono jet + missing transverse energy (\cancel{E}_T), mono b-jet + \cancel{E}_T , and top quark(s) + \cancel{E}_T channels. Model-independent upper limits (expected limits) on the cross section times acceptance for non-standard model events are derived at 7 TeV (8 or 14 TeV) running of the LHC experiment. With assuming that the dark matter is a singlet real scalar or a singlet Majorana fermion, we also put constraints on several operators describing its interactions with up, down, strange, charm, bottom and top quarks. These constraints are compared to those obtained by cosmological and astrophysical observations of the dark matter.

1 Introduction

The origin of the dark matter in the Universe and its nature are the most outstanding mysteries in modern particle physics, cosmology, and astrophysics. Though the problem is not resolved yet, many theoretical and experimental efforts have been made to search for the dark matter, and those give precious information about several dark matter interactions. Theoretically, the weakly interacting massive particle (WIMP) is one of the promising candidates for dark matter [1] and the couplings of the interactions involving the WIMP are predicted to be of the order of the electroweak (EW) couplings. Experimentally, direct detection experiments of dark matter put very severe limits on the scattering cross section between the dark matter and a nucleon [2], while indirect detection experiments give constraints on self-annihilation cross sections of the dark matter into various final states [3].

Among dark matter interactions, those to quarks and gluons are particularly well investigated thanks to the Large Hadron Collider (LHC) experiment. Importantly, the LHC experiment enables us to explore not only the interactions relevant to direct and indirect dark matter detections but also the interactions irrelevant to those detections. According to this fact, many studies have already been performed assuming a definite relation among the dark matter interactions with various quarks or using an analysis with simple collider simulations [4]. In this article, we thoroughly investigate present and (near) future expected limits on the dark matter interaction with each quark with focusing on mono jet + missing transverse energy (\cancel{E}_T), mono b-jet + \cancel{E}_T , and top quark(s) + \cancel{E}_T channels, which are all derived from dedicated collider simulations with use of a model-independent method.

In the next section (section 2), we first summarize dark matter interactions assuming that the dark matter particle is a real scalar or a Majorana fermion which is singlet under SM gauge groups. These dark matter candidates are frequently used in many literatures and can be regarded as the simplest example of a dark matter particle. We then put limits on the operators from cosmological and astrophysical observations of the dark matter in section 3. We next consider what kinds of dark matter signals are generally expected at the LHC experiment in section 4 and give model-independent upper limits (expected limits) on the cross section times acceptance for dark matter signals at 7 TeV (8 or 14 TeV) run. It turns out that these limits are very useful to constrain any dark matter quark interactions. Using the obtained limits, we also explain how to put a limit on each operator (discussed in

section 2) describing a dark matter interaction with various quarks. We finally consider how severely the LHC experiment can put limits on those operators in section 5 and compare the limits with those obtained from the cosmological and astrophysical observations. Section 6 is devoted to a summary of our discussions.

2 Dark matter interactions

Dark matter interactions with various quarks are discussed in this section assuming that the dark matter is a real scalar or a Majorana fermion which is singlet under SM gauge groups. We introduce operators describing interactions between the dark matter and SM particles up to the mass-dimension of six. Decoupling and/or weakly coupled heavy physics behind the interactions are implicitly assumed, so that the whole theory is renormalizable. Because of the stability of the dark matter, which is guaranteed by imposing a Z_2 symmetry, the operators have to involve two dark matter fields. The real scalar dark matter is denoted by ϕ , while the Majorana fermion dark matter is denoted by χ in following discussions.

The effective lagrangian for the scalar dark matter field ϕ is simply given by

$$\mathcal{L}_{\text{eff}}^{(\phi)} = \mathcal{L}_{\text{SM}} + \left[\frac{1}{2} (\partial\phi)^2 - \frac{M_\phi^2}{2} \phi^2 \right] + \sum_{n=4}^{\infty} \frac{1}{\Lambda^{n-4}} \left[\sum_i c_i \mathcal{O}_i^{(n)} + h.c. \right], \quad (1)$$

where \mathcal{L}_{SM} is the SM lagrangian and M_ϕ is the invariant mass term of the dark matter. Since several interactions will contribute to the dark matter mass after the electroweak symmetry breaking, we use the notation m_ϕ to describe the physical dark matter mass throughout this paper. The mass dimension of operator $\mathcal{O}_i^{(n)}$ is denoted by n , while Λ is the cutoff scale. The effective lagrangian describes the physics below the scale. The complete set of higher dimensional operators, which are invariant under both Lorentz group and SM gauge groups, is given by

$$\begin{aligned} \mathcal{O}_{\phi H}^{(4)} &= \phi^2 |H|^2, & \mathcal{O}_{\phi LHE}^{(6)} &= \phi^2 \bar{L} H E, \\ \mathcal{O}_{\phi H}^{(6)} &= \phi^2 |H|^4, & \mathcal{O}_{\phi QHD}^{(6)} &= \phi^2 \bar{Q} H D, \\ \mathcal{O}_{\phi \partial H}^{(6)} &= \phi^2 |D_\mu H|^2, & \mathcal{O}_{\phi QHU}^{(6)} &= \phi^2 \bar{Q} H^c U, \\ \mathcal{O}_{\phi VV}^{(6)} &= \phi^2 V_{\mu\nu} V^{\mu\nu}, & \mathcal{O}_{\phi V\tilde{V}}^{(6)} &= \phi^2 V_{\mu\nu} \tilde{V}^{\mu\nu}, \end{aligned} \quad (2)$$

where $H, L = (\nu, e_L)^T$, $E, Q = (u_L, d_L)^T$, D , and U are the higgs doublet, the lepton doublet, the charged lepton singlet, the doublet quark, the down-type singlet quark, and the up-type singlet quark, respectively. On the other hand, $V_{\mu\nu}$ ($\tilde{V}_{\mu\nu} \equiv \epsilon_{\mu\nu\alpha\beta} V^{\alpha\beta}$)

is the field strength tensor of a gauge boson, namely, $V_{\mu\nu} = B_{\mu\nu}$, $W_{\mu\nu}^a$, and $G_{\mu\nu}^a$ are those of the hyper-charge gauge boson, the weak $SU(2)_L$ gauge boson, and the gluon, respectively. The covariant derivative is denoted by D_μ . Operators $\mathcal{O}_{\phi LHE}^{(6)}$, $\mathcal{O}_{\phi QHD}^{(6)}$, and $\mathcal{O}_{\phi QHU}^{(6)}$ are in fact flavor-dependent such as $\phi^2 \bar{Q}_i H D_j$. In order to avoid dangerous flavor changing processes, we only consider flavor diagonal parts of the operators. This means that we are implicitly assuming that heavy physics has some mechanism to suppress flavor off-diagonal parts of the operators.

Since we are interested in interactions between dark matter and various quarks, we are focusing on $\mathcal{O}_{\phi Q_i HD_i}^{(6)}$ and $\mathcal{O}_{\phi Q_i HU_i}^{(6)}$ ($i = 1, 2, 3$) among the operators listed above. After the electroweak symmetry breaking ($\langle 0|H|0\rangle = (0, v)^T/\sqrt{2}$ with v being about 246 GeV), these operators give following effective interactions,

$$\mathcal{L}_{\text{int}}^{(\phi)} = \frac{v\phi^2}{\sqrt{2}\Lambda^2} \sum_{i=1}^3 \left[\bar{u}_i \left(c_{\phi Q_i HU_i}^{(R)} + i c_{\phi Q_i HU_i}^{(I)} \gamma_5 \right) u_i + \bar{d}_i \left(c_{\phi Q_i HD_i}^{(R)} + i c_{\phi Q_i HD_i}^{(I)} \gamma_5 \right) d_i \right], \quad (3)$$

where $c_{\phi Q_i HU_i}^{(R)}$ ($c_{\phi Q_i HU_i}^{(I)}$) and $c_{\phi Q_i HD_i}^{(R)}$ ($c_{\phi Q_i HD_i}^{(I)}$) are real (imaginary) parts of the coefficients $c_{\phi Q_i HD_i}$ and $c_{\phi Q_i HU_i}$ in front of the operators $\mathcal{O}_{\phi Q_i HD_i}^{(6)}$ and $\mathcal{O}_{\phi Q_i HU_i}^{(6)}$.

As in the case of the real scalar dark matter field ϕ , the effective lagrangian for the Majorana fermion dark matter field χ is also given in the same form,

$$\mathcal{L}_{\text{eff}}^{(\chi)} = \mathcal{L}_{\text{SM}} + \frac{1}{2} \bar{\chi} (i \not{\partial} - M_\chi) \chi + \sum_{n=5}^{\infty} \frac{1}{\Lambda^{n-4}} \left[\sum_i c_i \mathcal{O}_i^{(n)} + h.c. \right], \quad (4)$$

where we adopt the four component notation of the Majorana field $\chi = \chi^c$ with the superscript 'c' being the charge conjugation. Invariant mass term of the χ field is denoted by M_χ , which is taken to be real by an appropriate redefinition of χ . We use the notation m_χ to describe the physical mass of the dark matter χ . The complete set of effective operators involving two dark matter fields is given by

$$\begin{aligned} \mathcal{O}_{\chi H,1}^{(5)} &= (\bar{\chi} \chi) |H|^2, & \mathcal{O}_{\chi U}^{(6)} &= (\bar{\chi} \gamma^\mu \gamma_5 \chi) (\bar{U} \gamma_\mu U) \\ \mathcal{O}_{\chi H,2}^{(5)} &= i (\bar{\chi} \gamma_5 \chi) |H|^2, & \mathcal{O}_{\chi D}^{(6)} &= (\bar{\chi} \gamma^\mu \gamma_5 \chi) (\bar{D} \gamma_\mu D) \\ \mathcal{O}_{\chi H}^{(6)} &= (\bar{\chi} \gamma^\mu \gamma_5 \chi) (H^\dagger i \overleftrightarrow{D}_\mu H), & \mathcal{O}_{\chi L}^{(6)} &= (\bar{\chi} \gamma^\mu \gamma_5 \chi) (\bar{L} \gamma_\mu L) \\ \mathcal{O}_{\chi Q}^{(6)} &= (\bar{\chi} \gamma^\mu \gamma_5 \chi) (\bar{Q} \gamma_\mu Q), & \mathcal{O}_{\chi E}^{(6)} &= (\bar{\chi} \gamma^\mu \gamma_5 \chi) (\bar{E} \gamma_\mu E). \end{aligned} \quad (5)$$

Because of the same reason as the scalar dark matter case, we focus on flavor diagonal parts of the operators $\mathcal{O}_{\chi Q}^{(6)}$, $\mathcal{O}_{\chi U}^{(6)}$, and $\mathcal{O}_{\chi D}^{(6)}$, which give following interactions,

$$\mathcal{L}_{\text{int}}^{(\chi)} = \frac{2\bar{\chi} \gamma^\mu \gamma_5 \chi}{\Lambda^2} \sum_{i=1}^3 \left[\bar{u}_i \gamma_\mu (c_{\chi U_i} P_R + c_{\chi Q_i} P_L) u_i + \bar{d}_i \gamma_\mu (c_{\chi D_i} P_R + c_{\chi Q_i} P_L) d_i \right], \quad (6)$$

where all coefficients $c_{\chi U_i}$, $c_{\chi D_i}$, and $c_{\chi Q_i}$ are real numbers.

3 Cosmological and astrophysical constraints

We are ready to put limits on each operator describing interactions between the dark matter and various quarks. In this section, we consider various limits obtained from cosmological and astrophysical observations. The current and future expected limits on the operators obtained from the LHC experiment will be discussed in the next section. For the real scalar dark matter ϕ , following twelve operators, $\phi^2 \bar{u}_i u_i$, $\phi^2 \bar{u}_i i \gamma_5 u_i$, $\phi^2 \bar{d}_i d_i$, and $\phi^2 \bar{d}_i i \gamma_5 d_i$ are considered, where index i runs from one to three. On the other hand, for the Majorana fermion dark matter χ , following nine operators, $(\bar{\chi} \gamma^\mu \gamma_5 \chi)(\bar{u}_i \gamma_\mu P_R u_i)$, $(\bar{\chi} \gamma^\mu \gamma_5 \chi)(\bar{d}_i \gamma_\mu P_R d_i)$, and $(\bar{\chi} \gamma^\mu \gamma_5 \chi)(\bar{u}_i \gamma_\mu P_L u_i + \bar{d}_i \gamma_\mu P_L d_i)$ are considered. Because new physics model generally involves several operators simultaneously with appropriate coupling constants, putting limits on each operator should be regarded as a toy model. With keep in mind this fact, we simply assume that the effective lagrangian has only one of the operators mentioned above and explain how to put a limit on each operator in this and next sections.

3.1 Cosmological limit

A cosmological limit is obtained from the thermal relic abundance of the dark matter [5]. When the annihilation cross section of the dark matter is smaller, the resultant abundance is larger, leading to the over-closure of the universe. We therefore obtain a lower limit on the coefficient of the operator from the cross section.

For the scalar dark matter ϕ having interactions $(v\phi^2/\sqrt{2}\Lambda^2)(c^{(R)}\bar{q}q + c^{(I)}\bar{q}i\gamma_5 q)$, where q represents a quark ($q = u_i, d_i$) with m_q being its mass, the annihilation cross section of the dark matter ϕ (times relative velocity v_{rel}) is evaluated to be

$$\sigma v_{\text{rel}}|_{\phi\phi} \simeq \frac{3v^2}{2\pi\Lambda^4} \left[(c^{(R)})^2 (1 - m_f^2/m_\phi^2)^{3/2} + (c^{(I)})^2 (1 - m_f^2/m_\phi^2)^{1/2} \right] + \mathcal{O}(\epsilon),$$

where $\epsilon = (s - 4m_\phi^2)/(4m_\phi^2)$. Using a semi-analytical formula for the dark matter abundance [6], we obtain a lower limit on the coefficient $\sqrt{c^{(R)}}/\Lambda$ or $\sqrt{c^{(I)}}/\Lambda$.

On the other hand, for the Majorana fermion dark matter χ having a interaction $(2c/\Lambda^2)(\bar{\chi} \gamma_\mu \gamma_5 \chi)(\bar{q} \gamma^\mu P_{R(L)} q)$, the annihilation cross section is given by

$$\sigma v_{\text{rel}}|_{\chi\chi} \simeq \frac{4c^2}{\pi\Lambda^4} (4m_\chi^2 \epsilon + 3m_f^2/2) \sqrt{1 - m_f^2/m_\chi^2}, \quad (7)$$

where $\epsilon = (s - 4m_\chi^2)/(4m_\chi^2)$ again. As in the case of the scalar dark matter, we obtain a lower limit on the coefficient \sqrt{c}/Λ using the same semi-analytical formula.

3.2 Astrophysical limit 1 (Direct detection)

Direct detection experiments of dark matter put a stringent limit on each operator when the operator contributes to the spin-independent scattering cross section between the dark matter and a nucleon. In this paper, we adopt the result of the XENON100 [2]. For the scalar dark matter ϕ , as shown in equation (3), there are two types of interactions; scalar and pseudo-scalar interactions. Since the pseudo-scalar interaction is not constrained, the operators of the scalar dark matter are limited only through the scalar interaction.

Using the formula discussed in reference [7], the spin-independent scattering cross section between the dark matter and a nucleon is given by the following formula when the dark matter couples to light quarks (u , d , and s quarks);

$$\sigma_{\text{SI}} = \frac{(c^{(R)})^2 v^2 m_N^4 f_{Tq}^2}{2\pi\Lambda^4(m_\phi + m_N)^2 m_q^2}, \quad (8)$$

where $m_N \simeq 940$ MeV is the nucleon mass, while f_{Tq} is the parameter determined by the hadron matrix element $\langle N|\bar{q}q|N\rangle$. The values of the parameters for u , d , and s quarks are $f_{Tu} \simeq 0.028$, $f_{Td} \simeq 0.028$, and $f_{Ts} \simeq 0.009$, respectively [8]. On the other hand, when the dark matter couples to heavy quarks (c , b , and t quarks), the formula of the spin-independent scattering cross section is changed to be

$$\sigma_{\text{SI}} = \frac{(c^{(R)})^2 2v^2 m_N^4 f_{TG}^2}{729\pi\Lambda^4(m_\phi + m_N)^2 m_q^2}. \quad (9)$$

The parameter f_{TG} is determined by the hadron matrix element $\langle N|G_{\mu\nu}^a G^{a\mu\nu}|N\rangle$ and its value is evaluated to be $f_{TG} \simeq 0.9431$ through the trace anomaly relation, namely $f_{Tu} + f_{Td} + f_{Ts} + f_{TG} = 1$. The essential reason why the scattering cross section depends on the gluon hadron matrix element is that the dark matter can be scattered with a nucleon through the interaction with gluons inside the nucleon, whose process is mediated by the one-loop diagram of the heavy quark.

On the other hand, for the Majorana fermion dark matter χ , all interactions with quarks come from the axial-vector interaction of the dark matter, namely $\bar{\chi}\gamma_\mu\gamma_5\chi$. Only the spatial components of the interaction are survived at the non-relativistic limit, so that the corresponding quark interaction becomes $\bar{q}\gamma^i\gamma_5q$. These operators therefore do not contribute to the spin-independent scattering cross section but contribute to the spin-dependent one. Since a limit from direct detection experiments through the spin-dependent interaction turns out to be much weaker than that from the LHC experiment, we do not consider the constraint in this article.

3.3 Astrophysical limit 2 (Indirect detection)

Another astrophysical limit is obtained by indirect detection experiments of dark matter. Several products from dark matter annihilations at the galactic halo, for example, gamma-rays, positrons, electrons, anti-protons, and anti-deuterons, are utilized to detect the dark matter. Among those, one of the reliable limits on the annihilation cross section of dark matter comes from the indirect detection experiment through gamma-ray observations. In particular, the observations from the galactic center and milky-way satellites currently give the most stringent limit. In this article, we put a limit on each operator according to reference [9], in which a limit on the dark matter annihilation cross section obtained by the gamma-ray observation from the galactic center at the Fermi-LAT experiment is presented.

Differential gamma-ray flux in a direction ψ originated in dark matter annihilations at the region around the galactic center is given by the following formula,

$$\Phi(\psi) = \frac{1}{4\pi} \frac{\sigma v_{\text{rel}}}{2m_{\text{DM}}^2} \left[\frac{dN_\gamma}{dE} \right] \int_{l.o.s} dl \rho^2(l), \quad (10)$$

where σ is the annihilation cross section with v_{rel} being the relative velocity between incident two dark matters, while m_{DM} is the dark matter mass. The mass density of dark matter (the dark matter profile) at the position l is denoted by $\rho(l)$. The square of the dark matter density profile is integrated over along the observed line-of-sight. In our analysis, we have used the "Cored ($R_c = 1\text{kpc}$)" dark matter profile, which is one of the profiles used in the reference and gives the most conservative limit on the annihilation cross section. The fragmentation function dN_γ/dE , which is nothing but the gamma-ray spectrum produced per annihilation, has been estimated using the PYTHIA code [11] for various final states like $u\bar{u}$, $s\bar{s}$, $b\bar{b}$, $t\bar{t}$, etc.

Using the observational result of the Fermi-LAT experiment, model independent upper limits on the quantity $(\sigma v_{\text{rel}}/m_{\text{DM}}^2) \times \int_{E_i}^{E_f} dE [dN_\gamma/dE]$ for various energy bins, $(E_i, E_f) = (0.3, 1)$, $(1, 3)$, $(3, 10)$, and $(10, 100)$ in GeV unit, are presented in the reference. The upper limit on the annihilation cross section, σv_{rel} , is therefore obtained when the dark matter mass and the fragmentation function are given. Because the dark matter velocity at the present universe is three orders of magnitude smaller than the speed of light, the annihilation cross section is expressed by the s-wave component only. For the scalar dark matter, this is expressed by

$$\sigma v_{\text{rel}} \simeq \frac{3v^2}{2\pi\Lambda^4} \left[(c^{(R)})^2 (1 - m_f^2/m_\phi^2)^{3/2} + (c^{(I)})^2 (1 - m_f^2/m_\phi^2)^{1/2} \right],$$

where the interaction of the dark matter is assumed to be $(v\phi^2/\sqrt{2}\Lambda^2)(c^{(R)}\bar{q}q + c^{(I)}\bar{q}i\gamma_5q)$. On the other hand, for the Majorana fermion dark matter χ , the s-wave component of the annihilation cross section is given by the following formula,

$$\sigma v_{\text{rel}} \simeq \frac{6c^2m_f^2}{\pi\Lambda^4} \sqrt{1 - m_f^2/m_\chi^2}. \quad (11)$$

The dark matter is assumed to have the interaction $(2c/\Lambda^2)(\bar{\chi}\gamma_\mu\gamma_5\chi)(\bar{q}\gamma^\mu P_{R(L)}q)$. Since the annihilation cross section is proportional to the fermion mass squared because of the helicity suppression, only the interactions involving the second and third generation quarks are constrained by the indirect detection experiment.

In this section, we have discussed the method to put limits on the dark matter operators using cosmological and astrophysical observations. Obtained limits on each operator are summarized in figure 3 for the real scalar dark matter and figure 4 for the Majorana fermion dark matter in section 5, where limits from cosmology, direct detection, and indirect detection experiments are shown as brown, green, and blue lines in both figures. Physical interpretation of the results are discussed in section 5 in comparison with the limits obtained from the LHC experiment.

4 Constraints from the LHC experiment

We first discuss possible signals of dark matter at the LHC experiment. Dark matter particles are pair-produced from quark-quark interactions through higher dimensional operators discussed in section 2. However, the mere pair production does not produce missing transverse energy (\cancel{E}_T) and cannot be seen at the experiment. For this purpose, we need to pair-produce dark matter particles in association with jets or photons. In this case, the dark matter pair recoils against the visible particles and produces \cancel{E}_T . The generic signature of dark matter production at the LHC experiment is thus \cancel{E}_T plus a few number of jets or photons.

In view of collider searches, we can divide the dark matter effective operators into three parts, i.e., the operators containing light quarks, bottom quarks and top quarks respectively. In the first case, we can pair-produce dark matter particles with gluon/quark radiations from initial quark/gluon legs and thus observe the signal in the mono-jet plus \cancel{E}_T channel. In the second case, we need two bottom quarks in the initial state that may come from the gluon splitting. This means, we may produce dark matter pair plus b jets. The dark matter interaction with top quarks is very

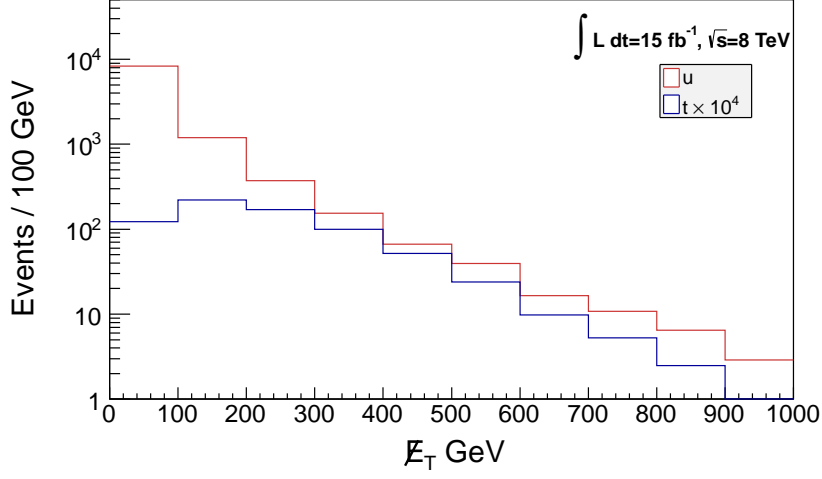


Figure 1: \cancel{E}_T distributions for the two operators described in the text at 8 TeV run.

different from two other cases. Here we need to produce two dark matter particles in association with two top quarks and the signal looks like top pair plus \cancel{E}_T . This final state is particularly interesting as it comes from different beyond the SM processes.

From above discussions, it is clear that the signals will be visible as events with \cancel{E}_T plus a few number of SM particles and the shape of the \cancel{E}_T distribution may be used to separate out those from SM backgrounds. However, unlike the R-parity conserving SUSY, \cancel{E}_T comes from the recoil of jets against dark matter particles and thus produces featureless rapidly decreasing distribution for dark matter coupled to light and bottom quarks. In case of top quark and dark matter effective operators, situation is slightly different as \cancel{E}_T can also come from semi-leptonic decays of W bosons. It is therefore important to compare \cancel{E}_T distributions for these two cases. The \cancel{E}_T distribution becomes harder with increasing the dark matter mass although the overall production cross section decreases with the mass.

For illustrative purpose, we take the two operators $(2\bar{\chi}\gamma^\mu\gamma_5\chi)(\bar{u}\gamma_\mu P_R u)/\Lambda^2$ and $(2\bar{\chi}\gamma^\mu\gamma_5\chi)(\bar{t}\gamma_\mu P_R t)/\Lambda^2$ assuming $m_\chi = 100$ GeV and $\Lambda = 1$ TeV. The \cancel{E}_T distribution is shown in figure 1 for 8 TeV run with 15 fb^{-1} integrated luminosity. It can be seen from the figure that, in case of top quark dark matter effective interaction, the \cancel{E}_T distribution is slightly harder compared to the light quark case although the cross section is extremely small. For this reason, it is not possible to probe such dark matter that couples very weakly to top quarks from current 8 TeV run and we have to consider high luminosity LHC run (100 fb^{-1}) with $\sqrt{s} = 14$ TeV.

4.1 Model independent upper limits

We now discuss model-independent upper limits on the cross section times acceptances for new physics interaction involving dark matter with three channels: mono jet + \cancel{E}_T , mono b-jet + \cancel{E}_T and top quark(s) + \cancel{E}_T searches. In order to estimate the prospects with 8 and 14 TeV runs of the experiment, we perform a Monte-Carlo (MC) simulation. Madgraph5 [10] is utilized to generate parton level events and the events are interfaced to PYTHIA6.420 [11] to deal with showering and hadronization. For detector simulation, we utilize Delphes2.0.2 [12] and resolution parameters are chosen based on the CMS detector performance given in reference [13].

4.1.1 Mono jet + \cancel{E}_T

The upper limit on the non-standard model contribution to the mono jet + \cancel{E}_T channel have already been reported in references [13, 14, 15] for 7 TeV run. In this paper, we take the results of reference [14] and set the constraints. We also estimate the prospect for 8 TeV run by the MC simulation imitating the search discussed in the reference. The basic selections used in the analysis are the following:

1. Event has the missing energy $\cancel{E}_T > 200$ GeV.
2. The leading jet has $p_T > 110$ GeV and $|\eta| < 2.4$.
3. The number of jets with $p_T > 30$ GeV is smaller than 3.
4. There is no isolated leptons or tracks with $p_T > 10$ GeV.
5. The second jet has $p_T < 30$ GeV or the difference of the azimuthal angle between the leading and the second jets is smaller than 2.5.

Here, notations p_T and η denote the transverse momentum and pseudo-rapidity respectively. In reference [14], with additional cuts $\cancel{E}_T > 250, 300, 350$, or 400 GeV applied, the upper limit on the number of the non-standard model events has been obtained. We express the results in terms of the cross section times the acceptance ($\sigma \times \mathcal{A}$), which are summarized in the table shown below;

Cut on \cancel{E}_T (GeV)	250	300	350	400
$\sigma \times \mathcal{A}$ (fb)	120	73.6	31.6	19.0

In order to estimate the prospect with the 8 TeV run as accurately as possible, we first perform the MC simulation with 7 TeV run and compare the background numbers with those of reference [14] and obtain normalization factors required to

	$W \rightarrow l\nu + \text{jets}$	$Z \rightarrow \nu\nu + \text{jets}$	$t\bar{t} + \text{jets}$
Cut 1-3	176369	62634	4756
Cut 4	157616	58216	4016
Cut 5	39084	56597	625
$\cancel{E}_T > 250 \text{ GeV}$	12915	21986	193
$\cancel{E}_T > 300 \text{ GeV}$	4950	9588	59
$\cancel{E}_T > 350 \text{ GeV}$	2065	4674	28
$\cancel{E}_T > 400 \text{ GeV}$	928	2337	20
$\cancel{E}_T > 450 \text{ GeV}$	473	1275	8
$\cancel{E}_T > 500 \text{ GeV}$	223	754	7

Table 1: *Cut flow table for the SM backgrounds at the mono jet + \cancel{E}_T channel. The center of mass energy of 8 TeV and the integrated luminosity of 15 fb^{-1} are assumed.*

adjust the difference. The same normalization factors are used to calculate the background for 8 TeV run. Note that the cross section obtained by MadGraph and PYTHIA is only at LO, and one needs K factor to obtain the correct normalization. Instead using the K factor, we compare our simulation to the distribution in the reference. As is shown in the reference, $W \rightarrow l\nu + \text{jets}$, $Z \rightarrow \nu\nu + \text{jets}$ and $t\bar{t} + \text{jets}$ are the dominant backgrounds, where l means the charged leptons. Other possible sources, QCD, single top, etc. are negligible. The cut flow for the standard model events is shown in table 1 assuming the integrated luminosity of 15 fb^{-1} .

We have calculated the expected 95% C.L. upper limit on the non-standard model cross section times the acceptance, which is summarized in the table below. Here, we have assumed that the systematic uncertainty associated with the estimation of the SM background events is 10%, which is same as the one in reference [14].

Cut on \cancel{E}_T (GeV)	250	300	350	400	450	500
$\sigma \times \mathcal{A}$ (fb)	459	191	89.1	43.6	23.7	13.7

4.1.2 Mono b-jet + \cancel{E}_T

The mono b-jet + \cancel{E}_T channel is expected to be useful to search for the dark matter which mainly couples to bottom quarks. In addition to the selection cuts used in the previous subsection (the cuts 1–5), we also require the following one:

6. The leading jet is b-tagged.

	$W \rightarrow l\nu + \text{jets}$	$Z \rightarrow \nu\nu + \text{jets}$	$t\bar{t} + \text{jets}$
$\cancel{E}_T > 350 \text{ GeV}$	33	111	23

Table 2: *Expected number of the SM events in the mono b-jet + \cancel{E}_T channel. The center of mass energy of 8 TeV and the integrated luminosity of 15 fb^{-1} are assumed.*

For the b-tagging method, we assume the following properties:

- The b-tagging efficiency is 0.6 for real b jets.
- The miss-tagging rate for light jet is 0.004.
- The miss-tagging rate for c-jet is 0.1.

These tagging efficiencies can be achieved in the CSVM tagger calibrated in reference [16]. In the case of the mono b-jet + \cancel{E}_T channel, we should not raise the cut on \cancel{E}_T as strong as that of the mono jet + \cancel{E}_T channel. For large \cancel{E}_T events, we expect large p_T for b-jets, which lower the efficiency of the b-tagging. For this reason, we just fix the cut on \cancel{E}_T to a moderate value ($>350 \text{ GeV}$) and set the constraint.

The estimation of the number of the SM events after the cuts 1–6 and $\cancel{E}_T > 350 \text{ GeV}$ is shown in table 2 for 8 TeV run assuming 15 fb^{-1} data. Here, “jets” also include the jets originate in heavy flavors. Since the mono b-jet + \cancel{E}_T channel is almost similar to the mono jet + \cancel{E}_T channel, the dominant backgrounds in the previous subsection are also the dominant ones here. We use the same normalization factor as the one in the mono jet + \cancel{E}_T channel to estimate the number of the events.

The expected 95% C.L. upper limit on the cross section times the acceptance for the non-SM event is estimated to be **2.9 fb**. Here, we have again assumed that the systematic uncertainty in the estimation of the SM events is 10%. One may expect that the use of tighter b-tagging condition efficiently reduces the W and Z backgrounds. However, it turns out that half of the remaining W and Z events include the real b-jets with the b-tagging properties we adopt. Therefore, tightening the b-tagging condition does not improve the result of our analysis.

4.1.3 Top quark(s) + \cancel{E}_T

Among the SM quarks, top quark needs separate treatment. It is heavy and not contained in protons. If the dark matter couples mainly to top quarks, dark matter production cross section is highly suppressed in comparison with the case with light quarks. In this case, the dark matter must be pair-produced associated with two top

quarks, and a top quark decays to hard b-jet, lepton, and neutrino that contributes to additional missing momentum. Therefore a specialized search strategy is required for such scenario. In this paper, we concentrate on the prospect for 14 TeV run because the production cross section is too small at 7 and 8 TeV runs.

The dominant background process to the top quarks + \cancel{E}_T channel is the $t\bar{t}$ production. The difference between the background process and the dark matter production in association with top quarks is that there is another source of \cancel{E}_T in addition to neutrinos from the leptonic decay of W boson. In order to suppress the SM $t\bar{t}$ events, we consider zero lepton mode in which the \cancel{E}_T from leptonic decay of W boson is suppressed. We therefore impose the following basic selection cuts:

1. There is neither isolated electron nor muon with $p_T > 20$ GeV.
2. There are at least four jets with $p_T > 100, 80, 50, 50$ GeV and one of them has to be b-tagged.
3. The azimuthal angles between the missing transverse momentum and the leading four jets are larger than 0.2.
4. $M_{\text{eff}} > 1000$ GeV and $\cancel{E}_T/M_{\text{eff}} > 0.3$.

M_{eff} is the scalar sum of the transverse momenta of the leading 4 jets and \cancel{E}_T .

Since the top quark(s) + \cancel{E}_T channel resembles the supersymmetry search with multi-jet + \cancel{E}_T [17], the dominant backgrounds are again $W \rightarrow l\nu + \text{jets}$, $Z \rightarrow \nu\nu + \text{jets}$ and $t\bar{t} + \text{jets}$. Interestingly, we find that M_T^R variable [18] is useful to separate out signals from SM $t\bar{t}$ events. In order to define the variable, we first define two mega jets. If n jets are present in the event, there are 2^{n-1} possibility for reconstructing two mega jets. Among them, we choose the one which minimize the sum of the square of the two mega jet masses. From the four momentum of the two jets p^{j1}, p^{j2} and the transverse missing momentum $\vec{\cancel{E}}_T$, M_T^R is defined by

$$M_T^R = \sqrt{\frac{\cancel{E}_T(p_T^{j1} + p_T^{j2}) - \vec{\cancel{E}}_T \cdot (\vec{p}_T^{j1} + \vec{p}_T^{j2})}{2}} \quad (12)$$

For the SM $t\bar{t}$ events, it is expected that M_T^R distribution has a cut off around m_t , while that of the signal is expected to be broader. We show M_T^R distributions for standard model $t\bar{t}$ and for dark matter effective operator $(2\bar{\chi}\gamma^\mu\gamma_5\chi)(\bar{t}\gamma_\mu P_R t)/\Lambda^2$ in figure 2 assuming $m_\chi = 100$ GeV and $\Lambda = 1$ TeV after imposing the selection cuts 1–3. Based on this distribution, we impose additional cuts $M_T^R > 300, 400, 500$,

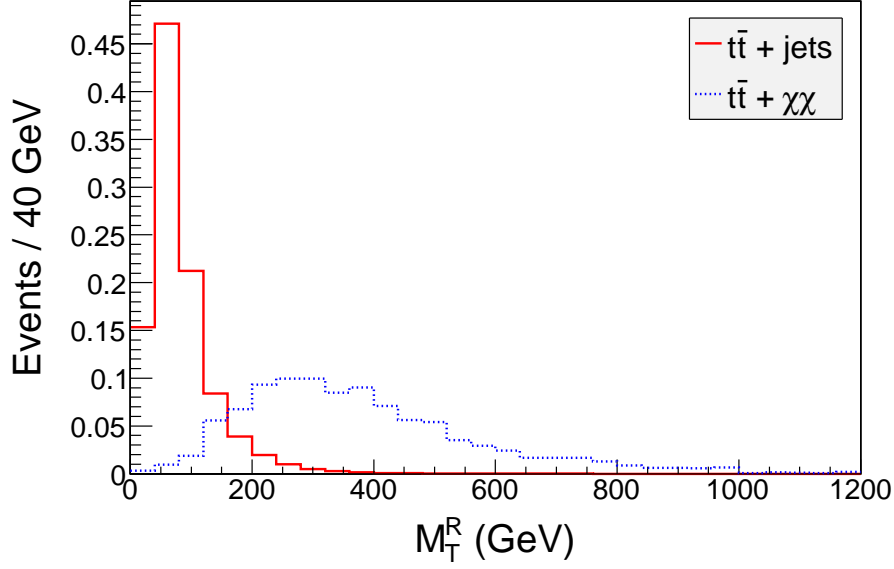


Figure 2: Normalized distribution of the M_T^R variable for the SM background ($t\bar{t}$) and for dark matter effective operator $(2\bar{\chi}\gamma^\mu\gamma_5\chi)(\bar{t}\gamma_\mu P_R t)/\Lambda^2$ events after imposing the selection cut 1–3. Center of mass energy of the LHC experiment is set to be 14 TeV.

600, 700, 800 and 900 GeV. The cut flow for the SM backgrounds, namely $t\bar{t}$ + jets, $W \rightarrow l\nu$ + jets, and $Z \rightarrow \nu\nu$ + jets backgrounds are shown in table 3.

As expected, the $t\bar{t}$ + jets background reduces drastically with M_T^R cuts applied, while Z and W backgrounds are not reduced significantly by this cut. Here, the number of the $t\bar{t}$ events is normalized assuming the total cross section of 920 pb [19]. The numbers of the $W \rightarrow l\nu$ + jets and $Z \rightarrow \nu\nu$ + jets events are normalized with the matched cross section obtained from the MadGraph-PYTHIA package. We have calculated the expected 95% C.L. upper limit on the non-standard model cross section times the acceptance, which is shown in the table below. Here, the systematic uncertainty in the estimation of the standard model events was assumed to be 10%, which is typical of the supersymmetry search with hadronic mode.

Cut on M_T^R (GeV)	300	400	500	600	700	800	900
$\sigma \times \mathcal{A}$ (fb)	12.2	10.2	4.57	1.87	0.839	0.418	0.208

In this paper, only the result for the hadronic mode has been shown. On the other hand, we also have estimated the prospects using the one (leptonic) and two lepton (semi-leptonic) modes. For the leptonic mode, we use the M_{T2} variable constructed from \cancel{E}_T and the transverse momentum of two leptons. For the semi-leptonic mode,

	$t\bar{t}$ +jets	$Z \rightarrow \nu\nu$ +jets	$W \rightarrow l\nu$ +jets
Cut 1-4	5746	258	176
$M_T^R > 300$ GeV	5723	255	176
$M_T^R > 400$ GeV	4753	239	174
$M_T^R > 500$ GeV	1934	200	141
$M_T^R > 600$ GeV	659	143	95
$M_T^R > 700$ GeV	239	85	50
$M_T^R > 800$ GeV	94	47	19
$M_T^R > 900$ GeV	21	21	14

Table 3: Expected cut flow for the SM backgrounds in the top + \cancel{E}_T channel. The center of mass energy of 14 TeV and the integrated luminosity of 100 fb^{-1} are assumed.

the M_T variable constructed from \cancel{E}_T and the transverse momentum of a lepton are used to reduce the background. These methods are discussed in reference [20], and those would be useful for the scalar top search. We find, however, that the constraints on the effective operators involving top quarks, which will be discussed in the next section, are weaker than the one with the hadronic mode.

We are now ready to discuss how we can put the current and future expected limits on each operator from the LHC experiment. For this purpose, we implement the interactions described in section 2 in Madgraph5 with the aid of Feynrules [21] and perform MC simulations for three channels as discussed above.

In order to put constraints on the operators involving light quarks (up, down, charm and strange quarks), we perform the mono jet + \cancel{E}_T analysis. We find the optimized cut on \cancel{E}_T by maximizing the ratio of the efficiency for accepting the signal to the upper bound on the cross section times the acceptance for the non-standard model events. For the reference point to obtain the optimized value, we choose the dark matter mass of 100 GeV and the interaction with up quark.¹ The results are summarized in table 4. We find that stronger cut on \cancel{E}_T gives more severe bound on the interactions for the Majorana fermion dark matter. It is possible that cut on \cancel{E}_T larger than the value we have shown in section 4.1.1 gives more severe bound. However, stronger cut will lead to larger systematic error thus we do not consider this possible improvement in this paper. The current and future expected constraints on

¹The optimized value do not change more than 50 GeV even if we choose other reference points.

	Real scalar	Majorana fermion
7 TeV	350 GeV	400 GeV
8 TeV	500 GeV	500 GeV

Table 4: *Optimized cut on \cancel{E}_T for the real scalar and the Majorana fermion dark matters.*

each operator are shown in the first and the second columns of figure 3 and 4 in the next section.

In order to put constraints on the operators involving bottom and top quarks, we perform the mono b-jet + \cancel{E}_T and the top quarks(s) + \cancel{E}_T analysis, respectively. For the top quarks(s) + \cancel{E}_T analysis, the optimized cut on M_T^R turns out to be 900 GeV for both the real scalar and the Majorana fermion dark matters. The future expected constraints on the operators are shown in the third columns of figures 3 and 4.

5 Results

In this section, we discuss limits on the dark matter effective operators mentioned in section 2. We have already explained in the previous two sections that the limits come mainly from WMAP, Fermi-LAT, XENON100 and LHC experiments. Since the structures of the operators are very different for the real scalar and the Majorana fermionic dark matters, we discuss the results of these two classes of interactions separately in following subsections. In all cases, we vary dark matter mass from 10 GeV to 1 TeV and calculate the limits and future prospects in terms of the combination of the cut-off scale (Λ) and the coupling (c), \sqrt{c}/Λ .

5.1 Scalar dark matter

Let us first discuss the (expected) limits for the real scalar dark matter interactions. All results are summarized in figure 3, where limits from cosmology, direct detection, and indirect detection experiments are shown as brown, green, and blue lines, while the current limit and future prospect from the LHC experiment are shown as magenta and pink lines, respectively. It can be seen that the limits obtained from the indirect detection are much stronger than those from the LHC experiment except for the operators $\phi^2 \bar{t}t$ and $\phi^2 \bar{t}\gamma^5 t$. This is because the production cross section at the LHC

experiment is small for the scalar dark matter, while its annihilation cross section is large as there is neither helicity nor p-wave suppression.

The limit from the direct detection experiment is also very strong for the scalar interactions, since they contribute to the spin-independent scattering cross section. The limit on the operator $\phi^2 \bar{c}c$ is stronger than that on $\phi^2 \bar{s}s$. The reason is the following. The hadron matrix element $\langle N | \bar{s}s | N \rangle$ is small ($f_{T_s} \simeq 0.009$), while the interaction with c quark is expressed by the interaction with gluons at low energy and the matrix element $\langle N | G_{\mu\nu}^a G^{a\mu\nu} | N \rangle$ is large ($f_{T_G} \simeq 0.9431$).

It is worth noting that the lines obtained from the cosmological limit are almost horizontal except the top quark mass threshold for the operators $\phi^2 \bar{t}t$ and $\phi^2 \bar{t}\gamma^5 t$. This is because the annihilation cross section of the scalar dark matter is controlled by the dimension-5 operator after the electroweak symmetry breaking, and the cross section depends very weakly on the dark matter mass.

It is also clear that the scalar interactions with u and d quarks are not favored from current data, whereas the interaction with top quark is the most difficult one to constrain. Even with 100 fb^{-1} data at 14 TeV run, it would be challenging to cover the most of the parameter space consistent with WMAP data.

5.2 Fermion dark matter

We next discuss the (expected) limits for the Majorana fermion dark matter. All results are summarized in figure 4, where the limits are shown in the same way as the scalar dark matter case. A remarkable point is that the limit from the indirect detection experiment is weak due to the helicity suppression. It is to be noted that the limit from the direct detection experiment is also very weak (and not shown in the figure), because the operators do not contribute to the spin-independent scattering cross section. It is therefore important to investigate the experimental way to search for the Majorana fermion dark matter at the LHC experiment.

The mono jet + \cancel{E}_T search gives strong limits on the dark matter interactions with light quarks (up, down, charm and strange quarks) in comparison with the limits obtained from the indirect detection experiment in the most of the parameter space, and so will the mono b-jet + \cancel{E}_T search on the interaction with bottom quark. Unfortunately, the limit from the 8 TeV run will not be much stronger than the one obtained in the 7 TeV run, since the number of SM background events increases as well as that of the signal events does. On the other hand, the top quark(s) +

\cancel{E}_T search will give comparable limits to those from the indirect detection for the interaction with top quark, which is a sharp contrast to the case of the real scalar dark matter.

6 Summary

We systematically investigate dark matter interactions with various quarks in the framework of effective operators. We consider the dark matter to be a singlet scalar or a Majorana fermion and thoroughly study bounds and future prospects of the dark matter discoveries from different astrophysical, cosmological and collider experiments. We have shown that the mono b-jet + \cancel{E}_T , and the top quark(s) + \cancel{E}_T channels along with the mono jet + (\cancel{E}_T) channel could be very important to search for the dark matter interacting with quarks. Here, we derive model-independent upper limits on the cross section times acceptance for these three channels mentioned above at 7 TeV (8 or 14 TeV) run of the LHC experiment. It is to be noted that the model independent bounds derived in our paper can also be used to constrain other dark matter or new physics models with similar type of signatures.

For the scalar dark matter with spin-independent interactions, the direct detection experiment supersedes the LHC bound because of smallness of the production cross section at the LHC experiment. In all cases whether it is spin-independent interaction or not, the indirect detection limit from Fermi-LAT data on the scalar dark matter is found to be stronger than the LHC bound. However, in case of the Majorana dark matter interactions considered in our work, the LHC experiment plays very important role for detection or exclusion of such possibility as the spin-independent cross section is zero. Possibility of detecting the top quark interaction with the dark matter is unfortunately not so promising at the LHC experiment even with 100 fb^{-1} data at 14 TeV run.

Acknowledgments

This work is supported by the Grant-in-Aid for Scientific research from the Ministry of Education, Science, Sports, and Culture (MEXT), Japan (Nos. 22244021, 23740169 for S.M., & Nos. 22540300, 23104006 for M.M.N.), and also by the World Premier International Research Center Initiative (WPI Initiative), MEXT, Japan. The work of K.H. is supported by JSPS Research Fellowships for Young Scientists.

References

- [1] G. Bertone, (ed.), Cambridge, UK: Univ. Pr. (2010) 738 p.
- [2] E. Aprile *et al.* [XENON100 Collaboration], arXiv:1207.5988 [astro-ph.CO].
- [3] O. Adriani *et al.* [PAMELA Collaboration], Phys. Rev. Lett. **105**, 121101 (2010);
M. Ackermann *et al.* [Fermi-LAT Collaboration], Phys. Rev. Lett. **107**, 241302 (2011).
- [4] Q. -H. Cao, C. -R. Chen, C. S. Li and H. Zhang, JHEP **1108**, 018 (2011);
M. Beltran, D. Hooper, E. W. Kolb, Z. A. C. Krusberg and T. M. P. Tait, JHEP **1009**, 037 (2010); J. Goodman, M. Ibe, A. Rajaraman, W. Shepherd, T. M. P. Tait and H. -B. Yu, Phys. Lett. B **695**, 185 (2011); S. Kanemura, S. Matsumoto, T. Nabeshima and N. Okada, Phys. Rev. D **82**, 055026 (2010);
J. Goodman, M. Ibe, A. Rajaraman, W. Shepherd, T. M. P. Tait and H. -B. Yu, Phys. Rev. D **82**, 116010 (2010); K. Cheung, K. Mawatari, E. Senaha, P. -Y. Tseng and T. -C. Yuan, JHEP **1010**, 081 (2010); P. J. Fox, R. Harnik, J. Kopp and Y. Tsai, Phys. Rev. D **85**, 056011 (2012); K. Cheung, P. -Y. Tseng, Y. -L. S. Tsai and T. -C. Yuan, JCAP **1205**, 001 (2012); P. J. Fox, R. Harnik, R. Primulando and C. -T. Yu, arXiv:1203.1662 [hep-ph].
- [5] E. Komatsu *et al.* [WMAP Collaboration], Astrophys. J. Suppl. **192**, 18 (2011) [arXiv:1001.4538 [astro-ph.CO]].
- [6] P. Gondolo and G. Gelmini, Nucl. Phys. B **360**, 145 (1991).
- [7] M. Drees and M. Nojiri, Phys. Rev. D **48**, 3483 (1993); G. Jungman, M. Kamionkowski and K. Griest, Phys. Rept. **267**, 195 (1996).
- [8] , *et al.* [JLQCD Collaboration], arXiv:1208.4185 [hep-lat].
- [9] D. Hooper, C. Kelso and F. S. Queiroz, arXiv:1209.3015 [astro-ph.HE].
- [10] J. Alwall, M. Herquet, F. Maltoni, O. Mattelaer and T. Stelzer, JHEP **1106**, 128 (2011).
- [11] T. Sjostrand, S. Mrenna and P. Z. Skands, JHEP **0605**, 026 (2006).
- [12] S. Ovnyn, X. Roubly and V. Lemaitre, arXiv:0903.2225 [hep-ph].
- [13] S. Chatrchyan *et al.* [CMS Collaboration], Phys. Rev. Lett. **107**, 201804 (2011).
- [14] S. Chatrchyan *et al.* [CMS Collaboration], arXiv:1206.5663 [hep-ex].
- [15] [ATLAS Collaboration], ATLAS-CONF-2012-084.

- [16] [CMS Collaboration], CMS-BTV-11-004.
- [17] G. Aad *et al.* [ATLAS Collaboration], arXiv:0901.0512 [hep-ex].
- [18] C. Rogan, arXiv:1006.2727 [hep-ph]; S. Chatrchyan *et al.* [CMS Collaboration], Phys. Rev. D **85**, 012004 (2012); [CMS Collaboration], CMS-SUS-11-008.
- [19] S. Moch and P. Uwer, Phys. Rev. D **78**, 034003 (2008).
- [20] T. Plehn, M. Spannowsky and M. Takeuchi, JHEP **1208**, 091 (2012).
- [21] N. D. Christensen and C. Duhr, Comput. Phys. Commun. **180**, 1614 (2009).

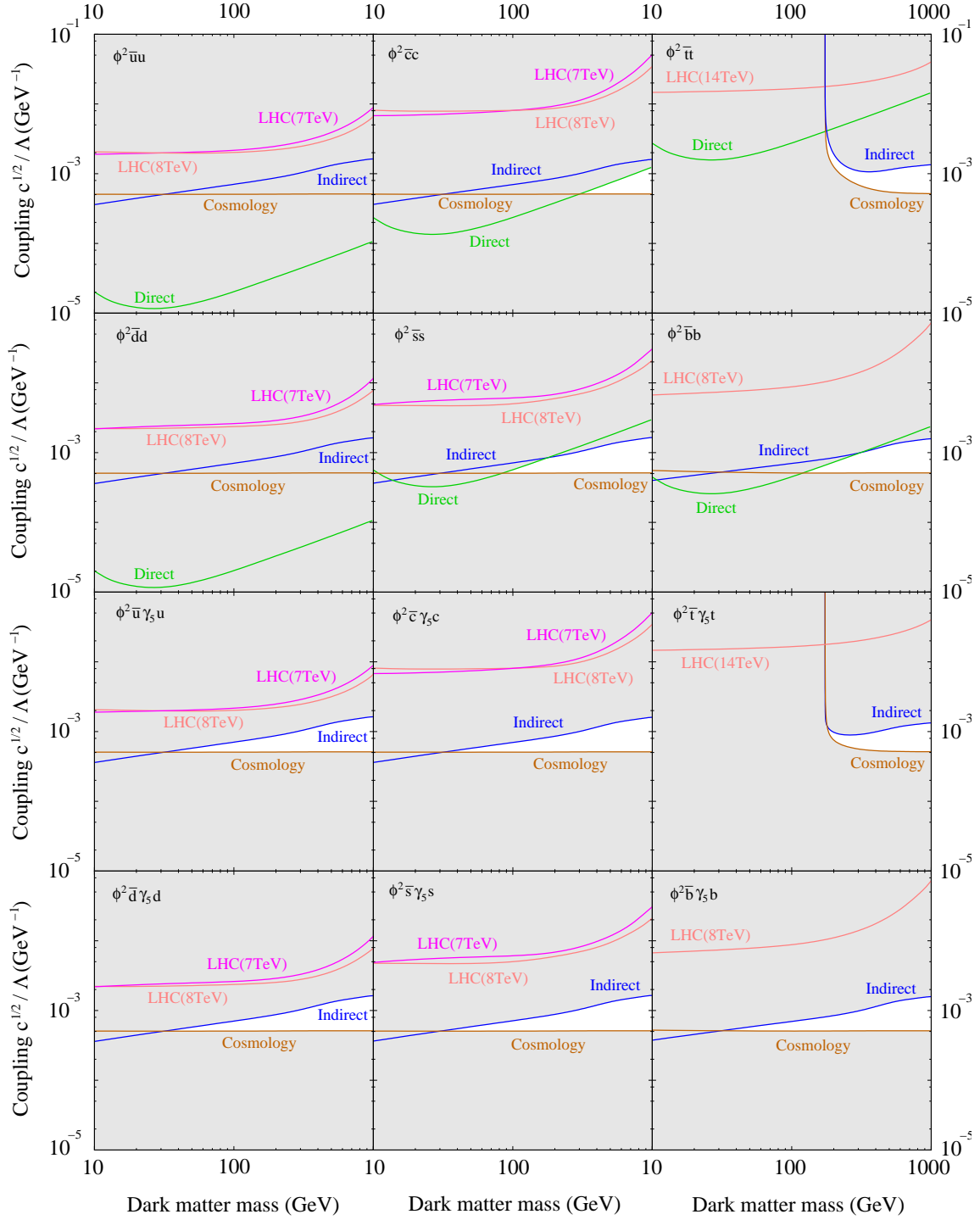


Figure 3: Limits on the operators describing the interactions between the real scalar dark matter ϕ and various quarks. Those from current LHC 'LHC(7TeV)', future LHC 'LHC(8TeV) & LHC (14TeV)', cosmological 'Cosmology', direct detection 'Direct', and indirect detection 'Indirect' experiments are shown as magenta, pink, brown, green, and blue lines, respectively in each panel of the figure.

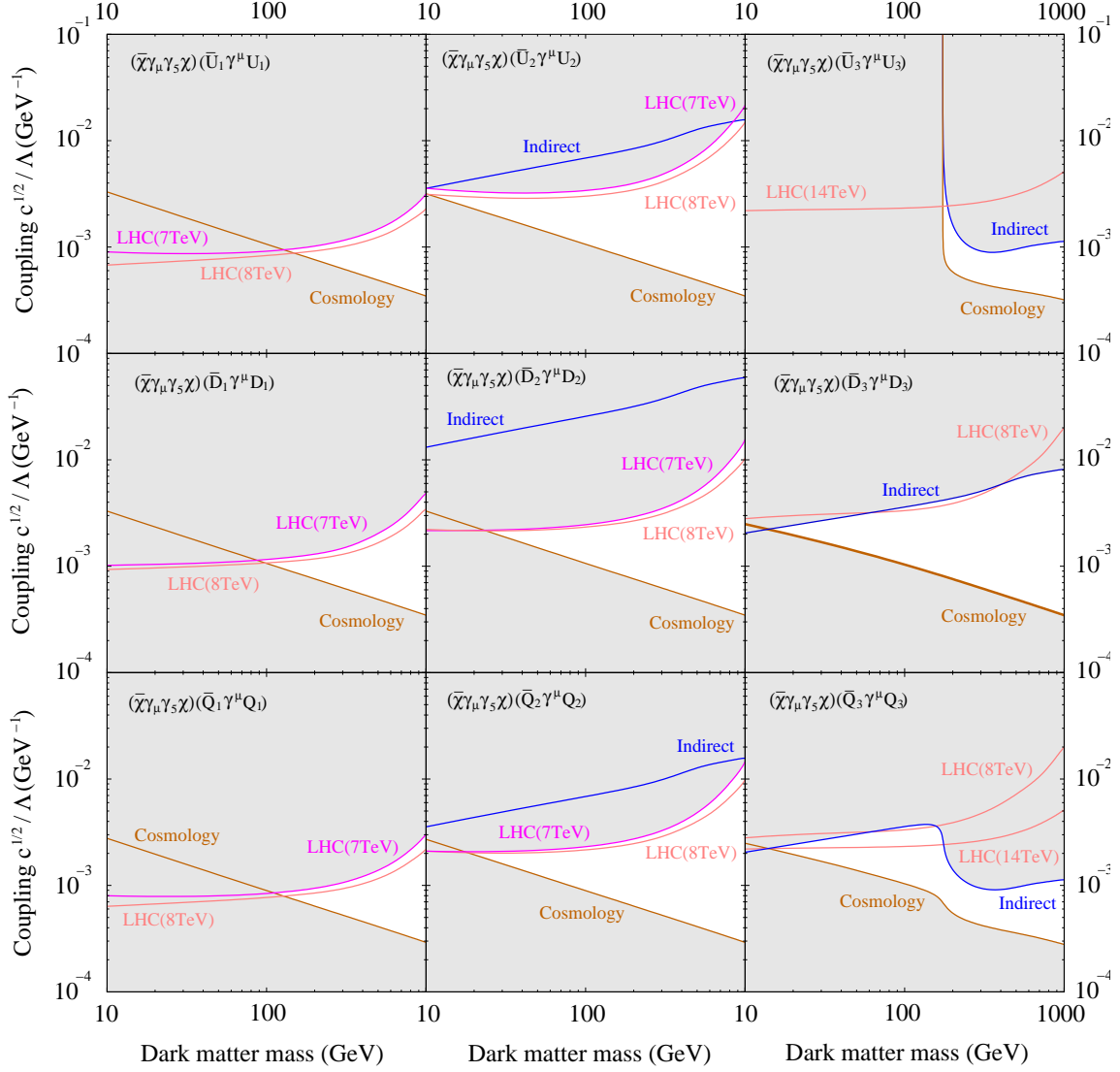


Figure 4: Limits on the operators describing the interaction between the Majorana fermion dark matter χ and various quarks. Those from current LHC 'LHC(7TeV)', future LHC 'LHC(8TeV) & LHC (14TeV)', cosmological 'Cosmology', direct detection 'Direct', and indirect detection 'Indirect' experiments are shown as magenta, pink, brown, green, and blue lines, respectively in each panel of the figure.